Carbon Combustion Synthesis of Complex Oxides: Process Demonstration and Features

K. S. Martirosyan and D. Luss
Dept. of Chemical Engineering, University of Houston, Houston, TX 77204

DOI 10.1002/aic.10528
Published online July 7, 2005 in Wiley InterScience (www.interscience.wiley.com).

Carbon combustion synthesis of oxides (CCSO) is a novel process to rapidly produce high-purity, submicron, and porous powders of complex oxides. It is a modified form of self-propagating high temperature synthesis (SHS) that uses carbon as the fuel instead of a pure metal. The CO_2 release increases the porosity and friability of the products. Like SHS, it is much faster (order of minutes) than the calcination processes (order of hours). CCSO has several advantages over SHS (the initial components are less expensive, porosity of the products is up to 70%). CCSO can produce complex oxides, such as $LaGaO_3$, which cannot be produced by SHS. The feasibility and features of CCSO are illustrated by its use in producing barium titanate, lithium manganese, and lanthanum gallium oxides. The carbon concentration enabled control of the moving front temperature and average velocity and the particle size and surface area. © 2005 American Institute of Chemical Engineers *AIChE J,* 51: 2801–2810, 2005
Keywords: oxides synthesis, gas–solid reactions, moving reaction front, carbon combustion, CCSO

Introduction

Because of their unique physical–chemical properties oxide ceramics have many important industrial applications, such as ferroelectrics, hard and soft magnetic ferrites, superconductors, optoelectronics, solid-oxide fuel cell components, battery electrode materials, catalysts, membranes, and pigments, to cite some of the primary uses.[1,2] The market demand for these oxides is continuously growing.[3]

Complex oxides can be synthesized by several processes that differ in the production price and product properties. The oldest and most common is calcination for 2–24 h in a furnace at a temperature of up to 1400°C.[4,5] In some cases, because of incomplete conversion the sintered material requires grinding and a second calcination. The process requires an expensive high-temperature furnace and high-energy consumption. Because of the long processing time at high temperatures, the particle size of the calcination products is often rather large, requiring extensive size reduction to enable manufacturing of the desired devices.

Several wet-chemical methods have been developed that produce more homogeneous products. They also provide better control of the particle size, which enables production of components with superior mechanical properties.[6] These techniques include coprecipitation,[7] sol–gel,[8] spray-drying,[9] aqueous combustion synthesis,[10,11] hydrothermal,[12] and cryochemical methods.[13] The wet-chemical methods require, in general, calcination at a high temperature to obtain a product with the desired composition and structure. Although the wet-chemical processes produce high-quality powders, the production costs are usually much higher than those in calcination.

Another method of producing oxides is *self-propagating high-temperature synthesis* (SHS), also referred to as combustion synthesis.[14-19] In this process a highly exothermic reaction between a metal powder (such as Fe, Ti, Zr, Al, Mg, Ni, Cu, Hf, Nb) and an oxidizer generates a high-temperature (order of 2000°C) front that propagates through the reactant mixture (velocity of 0.5–50 mm/s) converting them to products. The solid-state reaction continues after the combustion front passage in the postcombustion zone. SHS may also be conducted

Correspondence concerning this article should be addressed to D. Luss at dluss@uh.edu.

in the thermal explosion mode, in which the reactants are heated uniformly and the combustion is simultaneously initiated on the whole surface of the sample. The particle size is smaller than that produced by calcination but larger than that attained in several of the wet-chemical methods. Reported synthesis of complex oxides by SHS include superconducting,[20-22] magnetic ferrites,[23-26] solid-oxide fuel cell components,[27-30] and catalysts.[31]

The major advantages of SHS of oxide materials are: (1) low external energy consumption and no need for a high temperature furnace; (2) a very short reaction time—the typical combustion front velocity is from a few millimeters to a few centimeters per second; (3) simplicity of the process and a versatile reactor that can be used to synthesize various oxides; (4) products often have superior properties over those synthesized by other methods; and (5) possible in situ densification to form desired parts or articles.

Although several industrial applications of SHS have been reported in Russia and Europe, only a few have been reported in the United States. One reason is the lack of familiarity of the U.S. industry with the process. Several other reasons prevented the application of SHS for some specific applications. For example, SHS involves the use of a pure metal as a combustion fuel. When the price of the metal is a large fraction of the whole reactant mixture, the production costs by SHS may exceed that by the calcination process, which may use less-expensive metal containing precursors, such as carbonates or oxides. Moreover, SHS cannot be used when the pure metal combustion is not highly exothermic, or when the pure metal is either highly pyrophoric (such as lanthanum or lithium) or melts at room temperature (such as gallium). In addition, melting of the metal or intermediate oxide phases during SHS may have a deleterious impact on the product homogeneity. In addition, when the reactants are hygroscopic it may be difficult to mix them adequately by ball milling, and preparation and storage of the metal powders may affect the reactivity of the combustion.

We describe here a novel, modified SHS process that maintains the advantages of SHS and circumvents some of its disadvantages. Specifically, it enables a more economical synthesis of complex oxides when the price of the pure metal is a large fraction of the whole reactant mixture. It also enables synthesis of some oxides that cannot be produced by SHS.

Moreover, it enables synthesis of powders having a smaller particle size and a higher surface area. We describe the application of the process to synthesize three complex oxide powders that have important industrial applications, and the dependency of the process and product properties on the reactants' composition and operating conditions.

Carbon Combustion Synthesis of Oxides (CCSO) Process

The price of the reactant mixture used by SHS may be reduced by use of a fuel that is much cheaper than the metal fuel, and a metal-containing precursor such as a carbonate or oxide that is less expensive than the pure metal. The experiments reported here show that carbon powder may replace the pure metal as the fuel in the combustion synthesis of various oxides. This novel method, which we refer to as *carbon combustion synthesis of oxides* (CCSO) is a modified form of the traditional SHS.[32] The reactant mixture used in the CCSO is usually less expensive than that used in SHS because, instead of a pure metal, it uses a less-expensive metal-containing precursor (such as oxide, carbonate, nitrate, etc.) and carbon. The CCSO may be used to produce oxides even when SHS cannot be applied, such as when the pure metal is pyrophoric (such as Li or La) or that it melts at room temperature (such as Ga), or when the metal heat of combustion is relatively low. In contrast to the common SHS, the combustion product (carbon dioxide) is not incorporated in the product and exits from the sample. Moreover, the lubricating properties of the carbon enhance the mixing by ball milling.

The carbon combustion synthesis of oxides consists of the following overall chemical reaction

$$\sum_{i=1}^{n} \mu_i X_i^{(s)} + \alpha \mathrm{C}^{(s)} + \beta \mathrm{O}_2^{(g)} = \sum_{j=1}^{m} P_j^{(s)} + \alpha \mathrm{CO}_2^{(g)} + Q \quad (1)$$

where

$$\alpha = \frac{x/12}{(100 - x)/\sum \mu_i M_i^{(s)}}$$

$X_i^{(s)}$ is a solid compound containing the metal needed to form the oxide (such as an oxide, super oxide, nitride, or carbonate, chloride, or oxalate, etc.); $M_i^{(s)}$ is a molecular weight of each i component; $P_j^{(s)}$ is a solid product; μ_I and β are stoichiometric coefficients; x is the carbon wt % in the mixture; and Q is the heat of the reaction. The superscripts (s) and (g) denote solid and gas, respectively. After local ignition, the exothermic reaction between carbon and oxygen ($\Delta H = -393.5$ kJ/mol) provides the heat for the solid reactions and heats the adjacent reactant layer. This generates a self-sustaining temperature wave that propagates through the reactant mixture. The combustion features (such as moving front maximum temperature and velocity) and product properties may be adjusted by the amount of carbon in the mixture of reactants. We describe below the synthesis of three oxides by CCSO and the corresponding process features. Two of the oxides, $BaTiO_3$ and $LiMn_2O_4$, may also be produced by SHS (using a fuel of titanium and manganese powder), whereas the lanthanum gallium oxide ($LaGaO_3$) cannot be produced by SHS.

Experimental System and Procedure

The CCSO was conducted by loading a loose mixture of reactant powders (relative densities of about 0.3) into a ceramic boat that was placed inside a cylindrical stainless steel vessel (ID: 70 mm; length: 60 mm) fed by oxygen at a flow rate of up to 10 L/min. An infrared transparent sapphire window on top of the vessel enabled viewing and recording of the sample surface radiation by a high-speed (60 frames/s) infrared camera (Merlin Mid InSb MWI8, Indigo Systems). The IR images were used to determine the temperature, shape, and average combustion front velocity. The local combustion temperature (T_c) was measured by inserting in the center of the sample an S-type (Pt–Rh) thermocouple of about 0.1-mm diameter. The thermocouple readings were recorded and processed using an Omega data-acquisition board connected to a PC.

To initiate the propagating temperature front the reactant

Table 1. Characteristics of the Reactants Used during Carbon Combustion Synthesis of Oxide Composites

Reagent	Purity (%)	Average Particle Size (μm)	Standard Deviation (μm)	Melting Point (°C)	Source
BaO	99.5	22	3.6	1923	Alfa Aesar
BaO_2	95.0	16	2.2	450	Aldrich
$BaCO_3$	98.0	18	2.7	1000–1200 (decomp.)	Aldrich
Mn_2O_3	98.0	5	0.8	940–1090 (decomp.)	Alfa Aesar
La_2O_3	99.9	0.03	0.01	2280	Aldrich
Ga_2O_3	99.99	0.8	0.12	1725	Aldrich
Li_2O	99.5	26	4.8	1453	Alfa Aesar
TiO_2	99.5	0.95	0.17	1870	Alfa Aesar
Carbon	96.0	0.04	0.01	3800	Alfa Aesar
Oxygen (extra dry)	99.99	—	—	—	Aeriform Corp.

mixture was locally ignited by an electrically heated coil. The green mixture consisted of 7–40 wt % carbon and noncombustible oxide precursors. The molar ratio among the reactants was set according to the stoichiometry of the desired product. The powder mixture of reactants was thoroughly mixed by ball milling for about 15 min. The properties of the reactants are listed in Table 1. The effluent gas composition was determined by a three-channel gas microchromatograph analyzer (Varian Star Workstation 4100).

The quenched front method[33] was used to determine the structural transformations and product conversion during the CCSO. These experiments were conducted in a 62-mm-high copper cylinder with a 20-mm conical hole at the top and a 1-mm tip at its bottom. The cylinder was made of two separable halves to enable characterization of the dependency of the chemical composition on the position in the cone. After ignition at the top, the front extinguishes before reaching the bottom of the cone. The quenching rate was estimated to be 10^3–10^4 K/s.

The composition and crystal structure of the products was determined by X-ray diffraction (XRD; Siemens D5000 diffractometer) with Cu–K_α radiation. Scans were taken in the range of $5° < 2\theta < 80°$ at 0.1° intervals. Particle morphologies and microprobe analysis were determined by scanning electron microscopy (SEM; JEOL JAX8600, Tokyo, Japan) of loose powder affixed to a graphite disk with colloidal graphite paste. Particle size distribution and the surface area of the synthesized powder were determined by a Coulter SA 3100 Brunauer–Emmett–Teller (BET) analyzer. Surface areas were determined by the BET and Langmuir methods.

Experimental Results

Carbon combustion synthesis of oxides was used to produce three oxides, which have important applications. Specifically, we used the CCSO to synthesize: ferroelectric barium titanate ($BaTiO_3$); lithium manganese oxide ($LiMn_2O_4$), a common 4V cathode material; and lanthanum gallium oxide ($LaGaO_3$) used in various fuel-cell components.

The CCSO of $BaTiO_3$

$BaTiO_3$ was produced by the CCSO using three different Ba-containing precursors, by the following reactions

$$BaCO_3 + TiO_2 + \alpha(C + O_2) = BaTiO_3 + (\alpha + 1)CO_2 \uparrow \quad (2)$$

$$BaO_2 + TiO_2 + 2.4C + 1.9O_2 = BaTiO_3 + 2.4CO_2 \uparrow \quad (3)$$

$$BaO + TiO_2 + 2.4(C + O_2) = BaTiO_3 + 2.4CO_2 \uparrow \quad (4)$$

The impact of the carbon concentration (up to 40 wt %) on the maximum reaction temperature and average front velocity during the CCSO of $BaTiO_3$ with $BaCO_3$ as the barium precursor (reaction 2) is shown in Figure 1. The stoichiometric coefficient α, in reaction 2, was 3 (equivalent to 11.5 wt % carbon in the reactant mixture) in all the experiments except those in Figure 1. A self-sustaining reaction was not attained when x, the carbon wt % in the reactant mixture was <7. The combustion proceeded in an unstable mode at x = 7–8 wt % and the front extinguished after moving for about 2–4 mm. A stable combustion mode, in which the combustion front propagated at a constant velocity, was attained for reactant mixtures with carbon wt % >8. The reaction front propagated at a relatively slow velocity of about 0.3–0.4 mm/s using a reactant mixture with 8–10 wt % carbon and formed a friable and porous product. Increasing the carbon concentration in the green charge increased the average front velocity and maximum temperature. The stable front motion, generated using 8–40 wt % of carbon, led to maximum temperatures of 900–1200°C, well below the melting temperature of the $BaTiO_3$ product (~1600°C) and of carbon (3550°C). The velocity

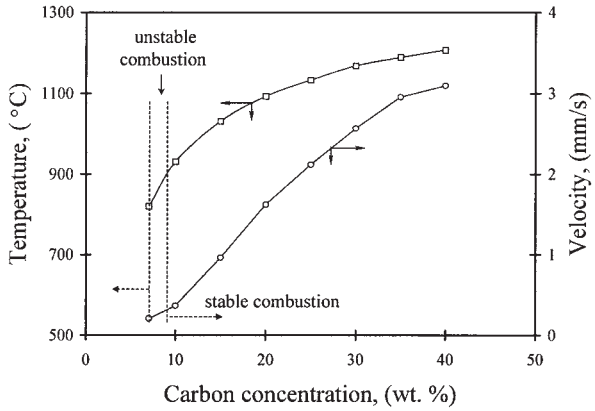

Figure 1. Influence of the carbon concentration in the green charge on the maximum reaction temperature and average front velocity and combustion regime during the carbon combustion synthesis of $BaTiO_3$ by reaction 2.

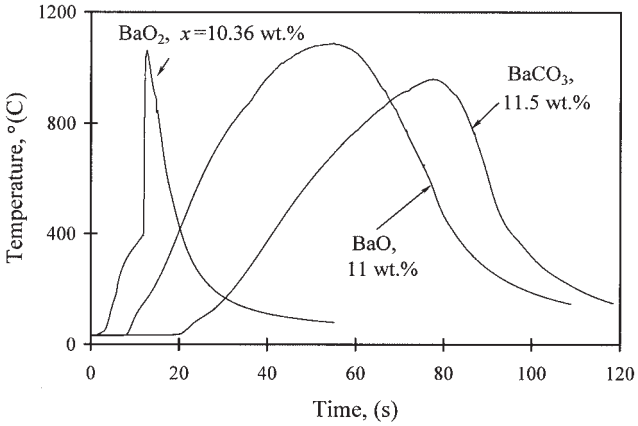

Figure 2. Typical temporal temperature at the center of the loose sample during the formation of $BaTiO_3$ by the CCSO with three different barium precursors (BaO, BaO_2, and $BaCO_3$).

x is the carbon wt % in the green charge.

approached an asymptotic value of about 3 mm/s and the maximum temperature an asymptotic value of about 1200°C at a carbon concentration of 40 wt %.

The temporal temperature at the center of the loose powder sample during the CCSO of $BaTiO_3$ by three different barium precursors (reactions 2–4) is shown in Figure 2. Using BaO_2 as the barium precursor (reaction 3 with $x = 10.36$ wt %), the temperature rapidly rose after the sample temperature reached 420°C. At this temperature the barium peroxide decomposed ($BaO_2 \rightarrow BaO + 0.5O_2$). The oxygen release increased the rate of the carbon combustion and the temperature rose at a rate of about 700°C/s. The corresponding combustion front propagated at an average velocity of about 0.4 mm/s and emitted a profusion of sparks. In contrast, when BaO was the barium precursor (reaction 4) the rate of the temperature rise was much lower, about 22°C/s, and the average velocity was 0.36 mm/s. When barium carbonate was the barium precursor (reaction 2 with $x = 11.5$ wt %), the temperature front velocity was 0.3 mm/s and the rate of the temperature rise about 16°C/s. The corresponding maximum combustion temperature of about 950°C was lower than that obtained using either BaO_2 or BaO as a barium precursor. The lower maximum temperature probably resulted from the heat consumed by the decomposition of the barium carbonate, $BaCO_3 \rightarrow BaO + CO_2$.

IR thermal images of the temperature during the CCSO of $BaTiO_3$ by reaction 4 are shown in Figure 3. They show that the moving temperature front was not exactly planar. The front propagated with an average velocity of about 0.36 mm/s and its maximum temperature was about 1120°C. The IR images did not show a clear boundary between the combustion zone and the postcombustion zone. The images suggest that the total reaction zone in the CCSO is wider (order of 15 mm) than that in conventional SHS.

To determine the dependency of the combustion temperature on the distance from the sample surface during reaction 4 we measured the temperature using four microthermocouples located at different depths within the sample. The total height of the loose mixture was about 30 mm. The maximum temperature of nearly 1080°C (same as that in Figure 2) was around the middle of the sample, at a distance of 15 mm from the surface. The smallest maximum temperature (~800°C) was generated on the bottom of the sample, close to the boat wall. The surface temperature was about 1000°C.

Experiments showed that the maximum temperature during the combustion of pure carbon was about 1300°C. The corresponding average front velocity was about 3.5 mm/s. Ignition of a mixture containing 11 wt % of carbon and $BaTiO_3$ generated a front with a maximum temperature of about 1100°C and a velocity of 0.32 mm/s. The combustion rate is limited by the rate of oxygen infiltration. The limiting reaction rate and the heat loss from the sample cause the temperature rise to be much smaller than the adiabatic temperature rise of carbon combustion.

The XRD patterns of the as-prepared $BaTiO_3$ product (Figure 4) indicate that the CCSO led to an almost complete conversion of the reactants to the perovskite-phase $BaTiO_3$ when either one of the two barium precursors (BaO and BaO_2) was used. The XRD patterns of the synthesized powders from these precursors have a flat background, indicating that amorphous reactants/intermediates/products were not present. The low-angle patterns do not include any "amorphous hump," which is indicative of the presence of amorphous material. Moreover, the sharpening of the diffraction peaks after a 1-h calcination at 1000 °C indicates that the product contains crystallites that grow on calcinations. In all XRD patterns of the products major reflection peaks corresponding to barium titanate ($BaTiO_3$) were observed. In the synthesis of $BaTiO_3$ using $BaCO_3$ as a precursor (Figure 4c) the combustion product contains some small amounts of barium and titanium oxides. Apparently, the incomplete reaction is caused by the difficult decomposition of barium carbonate. The reaction was com-

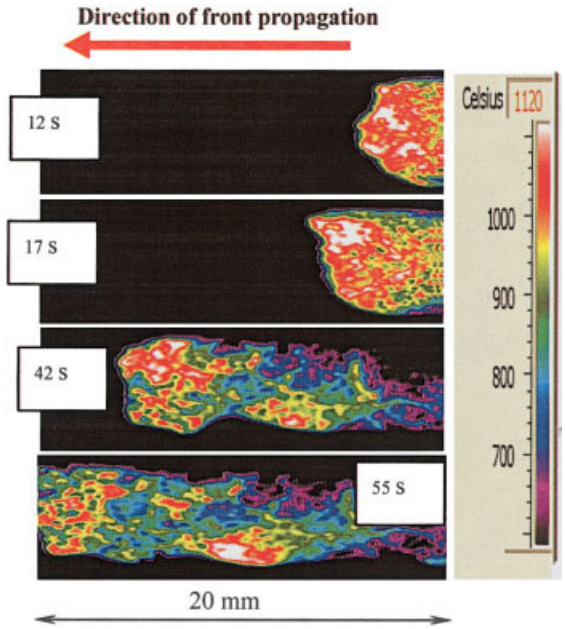

Figure 3. IR thermal images obtained during the carbon combustion synthesis of barium titanate $BaTiO_3$ by reaction 2.

Maximum combustion temperature: 1120°C; average front velocity: 0.36 mm/s. Mixture of reactants contained: 58.51 wt % BaO; 30.49 wt % TiO_2; and 11 wt % C.

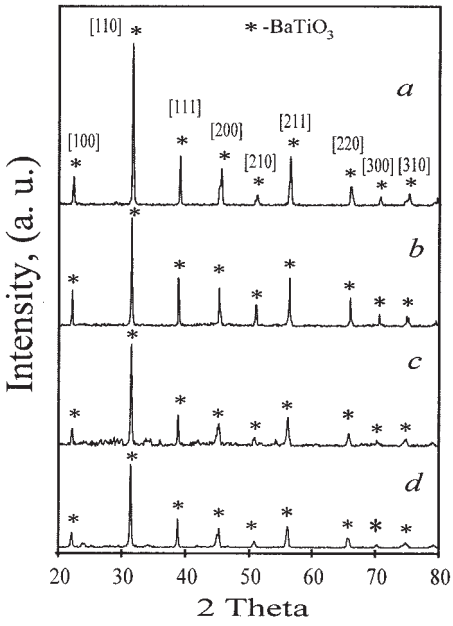

Figure 4. X-ray powder diffraction patterns of $BaTiO_3$ obtained after: (a) the calcination (1000° C, 1 h) of combustion products synthesized using BaO as a precursor; the CCSO using three different Ba precursors: (b) BaO, (c) $BaCO_3$, and (d) BaO_2.

The major diffraction peaks are of barium titanate.

pleted after a 1-h calcination of the product at 1000°C. The product was a pure, single-phase $BaTiO_3$. X-ray patterns of the product produced by reaction 4 using three different carbon concentrations (8, 20, and 30 wt %) in the green charge identified only $BaTiO_3$. The microprobe analysis confirmed that in all the experiments the product was $BaTiO_\gamma$, where $\gamma = 3 \pm 0.1$.

The characteristic microstructure of the barium titanate powder produced by the CCSO for three precursors and different carbon concentrations is presented in Figure 5. The average product particle size was about 0.2–1 μm for all precursors when a low carbon concentration of 8–11.5 wt % was used (Figures 5a–5d). Higher magnification of these samples shows that the agglomerates contained small particles with a smooth surface. The carbon combustion caused considerable gas (carbon dioxide) evolution, which generated many pores so that the synthesized powders became friable (porosity of the products was up to 70%) and loosely agglomerated. Increasing the carbon concentration up to 30 wt % decreased the fraction of the submicron particles and increased the pore size. The product was always spongy and the microstructure was homogeneous. After milling under identical conditions for 60 min, the surface area of barium titanate produced by the CCSO was 3.6 and 1.1 m^2/g, using mixtures with carbon concentrations of 11.5 and 30 wt %, respectively. The lower combustion temperature obtained at lower carbon concentrations (950°C with 11.5 wt % of carbon) apparently produced particles with smaller size and thus larger surface area.

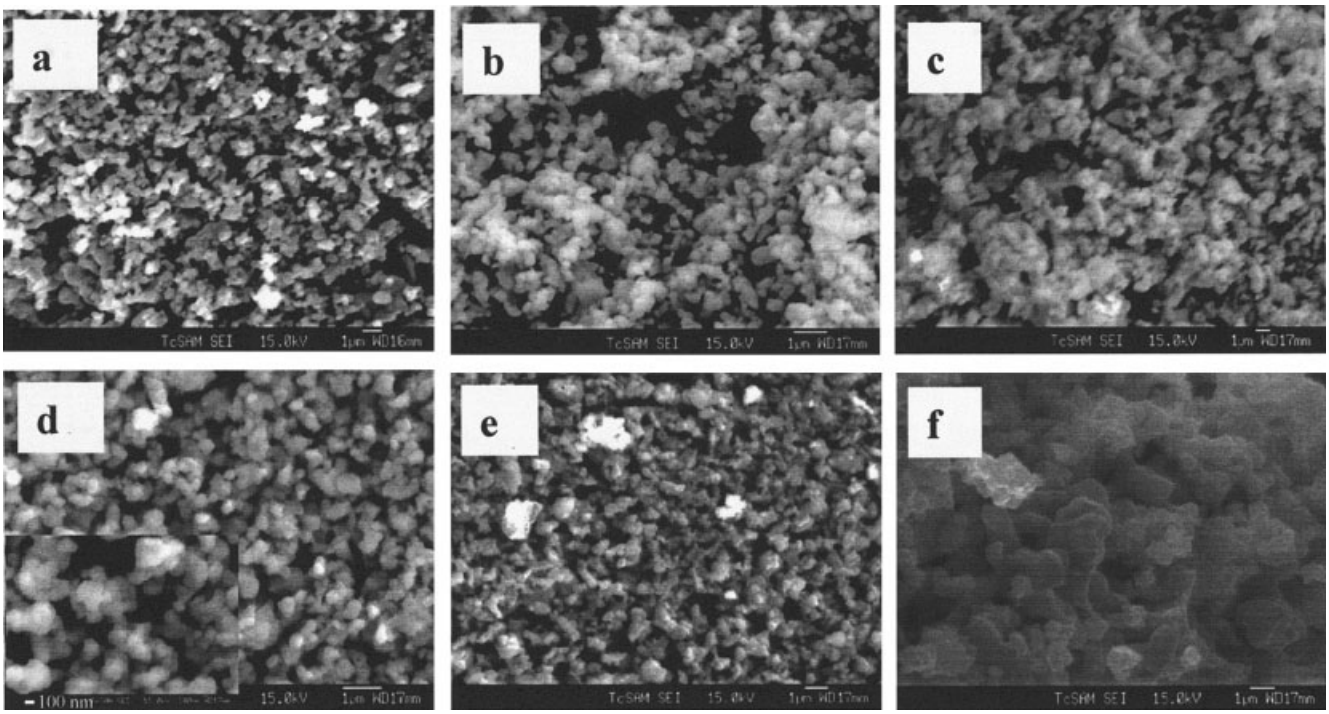

Figure 5. Characteristic microstructure (SEM images) of as-synthesized $BaTiO_3$ powders produced by carbon combustion synthesis by: (a–c) reactions 2, 3, and 4, respectively; (d–f) using $BaCO_3$ as a barium precursor with carbon concentration of (d) 8 wt %, (e) 20 wt %, and (f) 30 wt %.

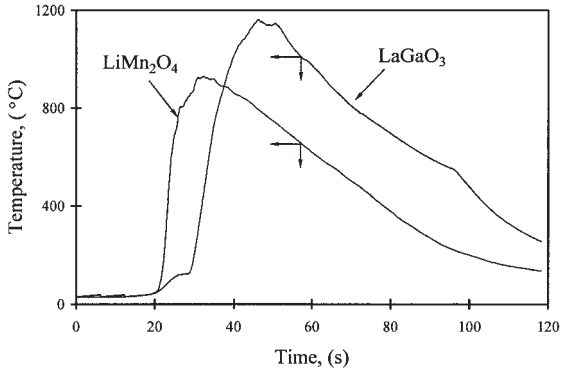

Figure 6. Local temporal temperature generated by carbon combustion synthesis of lithium manganese and lanthanum gallium oxide by reactions 5 and 6, respectively.

The CCSO of $LiMn_2O_4$ and $LaGaO_3$

The CCSO was used to produce $LiMn_2O_4$ and $LaGaO_3$ by the following reactions

$$Mn_2O_3 + 0.5Li_2O + 2C + 2.25O_2 = LiMn_2O_4 + 2CO_2 \uparrow \quad (5)$$

$$La_2O_3 + Ga_2O_3 + 4.5(C + O_2) = 2LaGaO_3 + 4.5CO_2 \uparrow \quad (6)$$

After ignition of the loose green charge for either reaction 5 or reaction 6 a stable combustion front propagated through the sample and converted the reactant mixture to the products. The IR thermal images of these reactions were similar to those during the CCSO of $BaTiO_3$. Figure 6 shows the temporal combustion temperature during the carbon combustion synthesis of lithium manganese and lanthanum gallium oxides. The maximum combustion temperature was about 920°C during the formation of $LiMn_2O_4$ and 1160 °C during that of $LaGaO_3$. The corresponding average combustion velocities were about 0.3 and 0.5 mm/s. The rate of the temperature rise by reaction 5 was about 100°C/s, whereas that during reaction 6 was slower, about 45°C/s. The maximum combustion temperatures in both cases were below the melting temperature of the products $LiMn_2O_4$ (>1000°C) and $LaGaO_3$ (~1700°C). Thus, the products were not affected by melting.

The microstructure of as-synthesized powders of lithium manganese and lanthanum gallium oxides, produced by reactions 5 and 6, is shown in Figure 7. Both products were friable with a spongy structure and composed mainly of agglomerated fine particles with a size of $\lesssim 1$ μm. The texture of the as-synthesized samples was homogeneous, consisting of many open pores.

Figure 8 is an XRD pattern of the combustion product $LiMn_2O_4$ obtained by reaction 5. The low-angle XRD and the wide-angle scans ($2\theta = 20-80°$) of the as-synthesized powder had a flat background, indicating that the combustion product was crystalline and no amorphous material was present. The XRD indicates that the synthesized powder was essentially pure $LiMn_2O_4$ with a cubic crystal structure. All the major

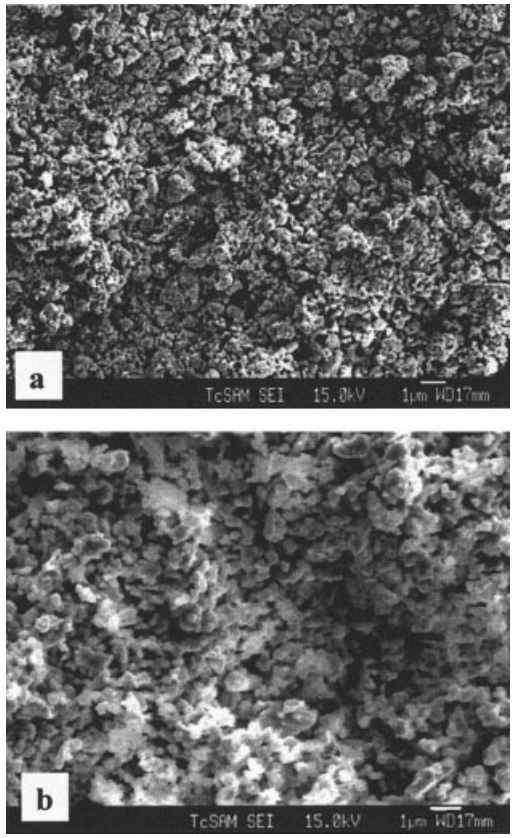

Figure 7. Microstructure of as-synthesized powders of (a) $LiMn_2O_4$ and (b) $LaGaO_3$ produced by carbon combustion synthesis.

diffraction peaks for as-synthesized and calcined powders were of lithium manganese oxide. The lack of diffraction patterns of other species indicates that the concentrations of any other crystalline species must be very low.

By use of the quenched front method, we followed the phase

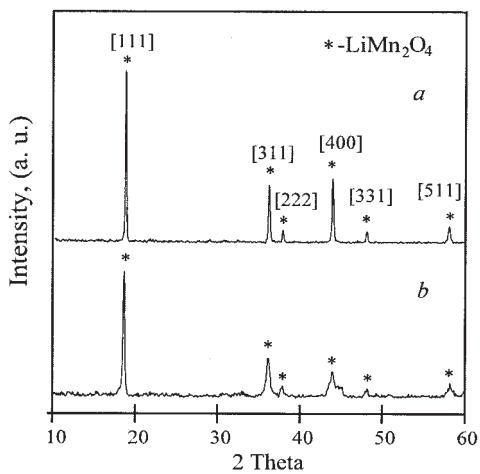

Figure 8. X-ray diffraction patterns of lithium manganese oxide ($LiMn_2O_4$): (a) after the calcination of the as-synthesized product at 1000 °C for 1 h; (b) as-synthesized powder.

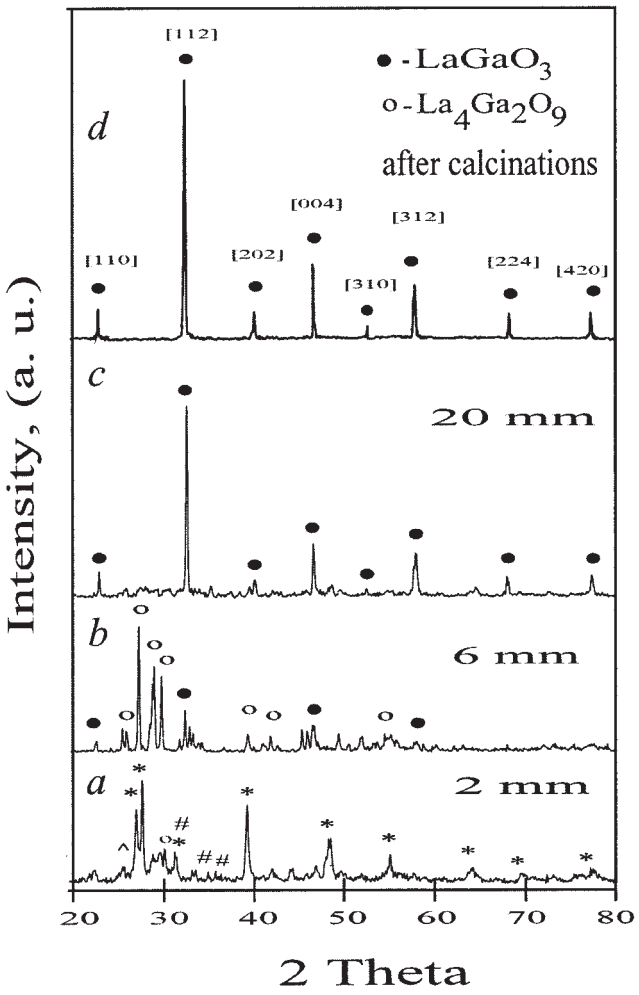

Figure 9. (a, b, c) X-ray powder diffraction patterns at various distances, from prefront plane in quench front experiment of the CCSO of $LaGaO_3$; (d) XRD after 1-h calcination of product at 1000°C.

Key: (*) La_2O_3; (#) Ga_2O_3; (^) C; (○) $La_4Ga_2O_9$ intermediate phase; (●) orthorhombic $LaGaO_3$. The major diffraction peaks of the product are of $LaGaO_3$.

and structural transformations occurring during the synthesis of lanthanum gallium oxide by carbon combustion synthesis. The sample in the conical copper cylinder was cut into two halves for analysis by XRD and microprobe. The combustion front, inside the copper cone, during the synthesis of $LaGaO_3$ by reaction 6 moved at a velocity of about 0.45 mm/s and was arrested at a distance of 1 mm from the tip of the cone. The combustion temperature in the middle of the sample rises to its maximum value of about 36 s. Thus, we estimate the average length of the total preheating and reaction zone at about 16 mm. Figure 9 shows some XRD patterns taken at a distance (l) from the prefront zone, chosen as the position at which the color of the green mixture began to change. The XRD pattern shows that La_2O_3 and Ga_2O_3 and carbon were mainly present in the combustion front zone at a distance of about 2 mm from the prefront zone. The diffraction peaks in that zone differ from those of the reactant mixture and of the final products and were of the intermediate $La_4Ga_2O_9$. The $LaGaO_3$ started to form in the combustion zone at a distance of about 6 mm from the prefront zone. Almost complete conversion of the reactant to the orthorhombic-phase $LaGaO_3$ was achieved in the postcombustion zone at a distance of 20 mm from the prefront line.

We note that, although lanthanum gallium oxide was produced by the CCSO, it cannot be synthesized by SHS using either La or Ga as the fuel because the lanthanum powder is highly pyrophoric and gallium powder melts at about 29°C.

Characterization of effluent gas

A potential health hazard associated with the CCSO is the generation of carbon monoxide. The effluent gas composition during the CCSO of barium titanate, lithium manganese, and lanthanum gallium oxide was determined by a three-channel gas microchromatograph analyzer. Typical data, shown in Figure 10, revealed that the effluent contained only oxygen and carbon dioxide. The partial pressure of CO_2 and O_2 was about 6.7 and 93.3%, respectively. No carbon monoxide CO was detected in the effluents during these CCSO. Evidently, some reactants and intermediate oxides catalyzed the complete conversion of the carbon to CO_2.

Discussion

Our experiments demonstrated the feasibility of producing complex oxides by the CCSO process, which is a modified SHS process in which the metal fuel is replaced by carbon. Similar to SHS, the features and stability of the self-propagating reaction during the CCSO depends on the heat generated by the carbon combustion reaction, enthalpy of phase transformation and reactions among the reactants, and the rate of the heat loss from the sample. A stable self-propagating reaction can be sustained only above a critical fuel (carbon) concentration. It was about 8 wt % in the synthesis of barium titanate (Figure 1).

Increasing the carbon concentration in the reactant mixture increased the moving front temperature and velocity, which eventually approach asymptotic values. This occurred when the carbon concentration was about 40 wt % in the synthesis of barium titanate. The asymptotic front temperature and velocity were close to values obtained during the combustion of carbon powder in oxygen. Because the maximum temperature during the CCSO did not exceed about 1250°C the CCSO did not cause melting of the desired products. The maximum temperature obtained in the CCSO depended on the metal containing precursors and the energy needed to decompose them. For example, the maximum temperature during the carbon combustion synthesis of $BaTiO_3$ was close to the decomposition temperature of barium carbonate precursor (Figure 2), which starts at about 1000°C.[34] It was pointed out by Hedval[35] that the decomposition temperature of carbonates may be significantly decreased by the presence of other oxides as a result of the increased ionic mobility and defect concentration on the particle surface. Thus, the presence of TiO_2 may have decreased the decomposition temperature of the barium carbonate.

Clearly the maximum temperature generated by the CCSO has to be sufficiently high to decompose the metal-containing precursors. This is not a limitation in most practical cases because this maximum temperature is similar to that used in conventional calcination processes to produce oxides (range of

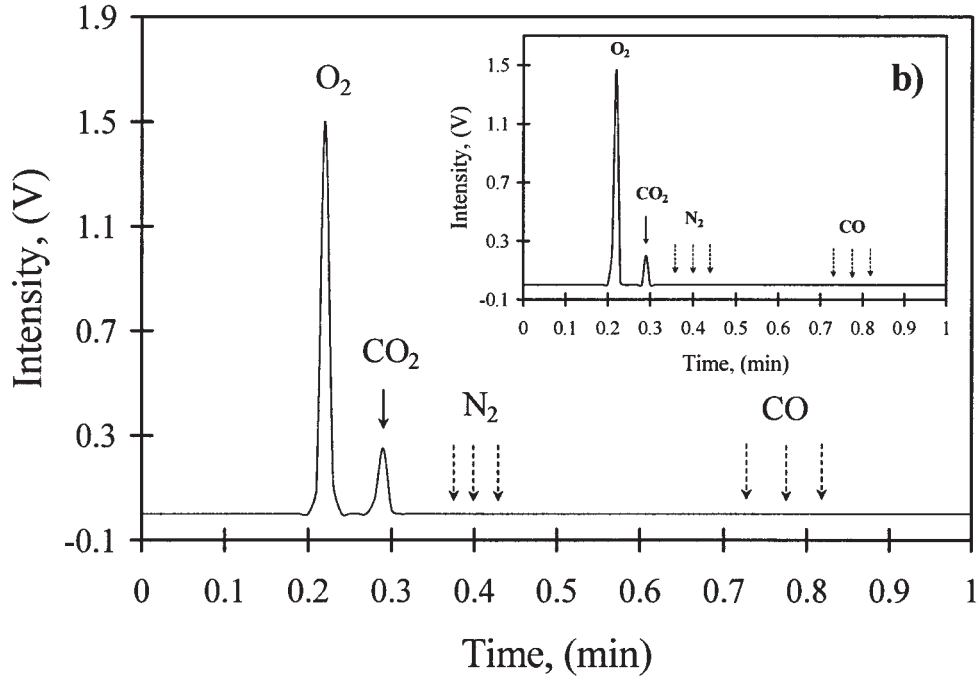

Figure 10. Chromatogram of the effluent gas during the carbon combustion synthesis of (a) $BaTiO_3$ by reaction 2; (b) $LaGaO_3$ by reaction 5.

Dotted arrows show the retention time of the nitrogen and carbon monoxide.

800–1200°C). Most metal-containing precursors, such as carbonates and nitrates, readily decompose in this temperature range. A major advantage of the CCSO over the calcination processes is that it is completed in a much shorter time and with a minimal energy input.

The maximal front temperatures and average velocity during the combustion of mixtures containing either BaO–TiO_2 or pure $BaTiO_3$ with about 11 wt % of carbon were approximately the same (~1100 °C and ~0.32 mm/s, respectively). This suggests that the heat of the reaction between BaO and TiO_2 to form barium titanate had a negligible impact on the front temperature and velocity. The typical rate of the temperature rise rates during the CCSO of different complex oxides were 16–100°C/s (using oxides or carbonates as a metal-containing precursor). The use of different barium precursors affected the rate of the net heat release by the reactions and the temperature rise during the synthesis of $BaTiO_3$ (Figure 2). Using $BaCO_3$ as the barium precursor led to the lowest rate of temperature rise (~16°C/s) because of its relatively slow decomposition. On the other hand, the active oxygen release by the decomposition of BaO_2 accelerated the combustion and led to a significantly higher rate of temperature rise (~700°C/s).

The length of the reaction zone in SHS is usually a few millimeters. A much wider reaction zone exists in the CCSO. For example, during the synthesis of $BaTiO_3$, the reaction zone length was about 15 mm (Figure 3). During the synthesis of lanthanum gallium oxide in the quenched front experiments it was about 16 mm. The larger length of the combustion zone can be explained by several effects. The temperature during SHS is usually higher and the rate of the metal combustion is much faster than that of the carbon combustion in the CCSO. Moreover, a slow decomposition rate of metal-containing precursor in the CCSO increases the time needed to complete the overall reaction.

As in SHS, increasing the sample size can lead to limitation of the gas infiltration rate into the sample and increase the temperature gradients within the sample. These factors affect the reaction front propagation velocity and cause the velocity, temperature, and conversion to depend on the distance from the sample surface. The release of the CO_2 in CCSO generates a more porous product than in traditional SHS. This increases the oxygen infiltration rate and minimizes its impact. The larger the sample size, the larger the temperature difference between the surface and the bottom of the sample and the impact of the oxygen infiltration. For example, a temperature difference of 280°C existed between the sample surface and sample bottom during reaction 4 and the reaction completion time of the barium titanate about doubled as the sample depth was increased from 10 to 30 mm. Although there is some critical sample depth above which the infiltration rate limitations will cause incomplete conversion of the carbon, this did not happen in any of our experiments using a sample depth of 30 mm.

An important feature of the CCSO is that an increase in the carbon concentration in the reactant mixture increases the front temperature and the product particle size and decreases the product surface area. Thus, variation of the carbon concentration enables control of the particle size and surface area. For example, during the CCSO of $BaTiO_3$ increasing the carbon concentration in the reactants mixture from 11.5 to 30 wt % increased the combustion temperatures from about 950 to about 1200°C and the average particle size from <1 to 5 μm, while decreasing the particle surface area from 3.6 to 1.1 m^2/g. Figure 5 clearly shows that a decrease in the maximum combustion

temperature decreases the product size and leads to a narrower particle size distribution.

The XRD patterns of the as-synthesized $BaTiO_3$ product (Figure 4) indicate that CCSO led to almost complete conversion, irrespective of which of the three different precursors was used. The single-phase products $BaTiO_3$, $LiMn_2O_4$, and $LaGaO_3$ synthesized by the CCSO (Figures 4, 8, and 9) were friable, with submicron particle size (Figure 5 and 7) and a high porous crystalline structure. The extensive CO_2 evolution during the carbon combustion most probably increased the porosity of the products. This, in turn, simplifies the particle size reduction by milling.

The carbon combustion synthesis of $LaGaO_3$ in the quenched front experiments shows that, similar to SHS, the CCSO proceeds in steps that involve production of intermediates. The experiments show that the decomposition of the precursor occurred very close (~2 mm) to the prefront zone. An intermediate product of $La_4Ga_2O_9$ formed well ahead of the combustion front. The formation of $LaGaO_3$ started when almost all the lanthanum and gallium oxides were consumed at a distance of about 6 mm from the prefront line. The transformation of the green mixture to $LaGaO_3$ was essentially complete at about 20 mm from the prefront line. The time to complete this reaction (~60 s) is much longer than the typical reaction time in SHS, which usually occurs at much higher temperatures.

An important concern involved in the CCSO is the possible formation of carbon monoxide. This did not occur and the effluent consisted of oxygen and carbon dioxide and no detectable carbon monoxide. Probably, any CO that formed was rapidly oxidized to CO_2 in the presence of the oxide precursors at the relative high reaction temperature (>900°C).

Our experiments demonstrate the ability of the CCSO to efficiently produce high-quality oxide powders that have important applications. The process has the same advantages as those of SHS: that is, it is rapid (order of 1–10 min), requires very simple and versatile equipment, requires minimal external energy input, and can be readily scaled-up for continuous operation. When the price of the metal is a significant fraction of that of the reactant mixture, the synthesis by the CCSO may be less expensive than that by SHS. Moreover, the CCSO may be used even under situations that SHS cannot be applied because of the pure metal being pyrophoric or melting at room temperature. Moreover, the lower temperature of the CCSO and the extensive release of CO_2 yield a product that has a lower particle size, a higher surface area, and is easier to mill. Our experiments indicate that carbon combustion synthesis of oxides has potential applications and that it is important to enhance our understanding of its features and its dependency on the feed composition and operating conditions.

Conclusions

The carbon combustion synthesis of oxides is a modified form of SHS, in which carbon is used as the fuel instead of a pure metal. The process has several advantages over SHS and can be applied even in cases in which it is not possible to produce the complex oxide by SHS. The process is significantly faster than the common calcination processes and produces powders with a smaller particle size. We used the method to successfully produce high-purity, submicron, and porous powders of barium titanate ($BaTiO_3$), lithium manganese ($LiMn_2O_4$), and lanthanum gallium oxide ($LaGaO_3$). The major parameters affecting the process are the carbon concentration in the reactant mixture and the metal containing precursor. A stable self-propagating reaction front can be obtained only at carbon concentrations exceeding a critical value. The reaction front temperature and average velocity increased as the carbon concentration in the reaction mixture increased, eventually approaching asymptotic values. The maximum combustion temperature (~1200°C) was close to that of a mixture of carbon and the products. The high rate of CO_2 release increases the porosity of the particles and the friability of the powder.

The experiments suggest that CCSO has the potential to enable a more economic and energy-efficient production of complex oxides, which have wide applications. The process is certainly capable of generating many complex oxides different from the three we produced. It is of practical importance and academic interest to gain better knowledge of the process and its dependency on the operating conditions and feed composition.

Acknowledgments

The authors acknowledge the financial support of this research by the National Science Foundation, the Texas Center for Superconductivity and Advanced Materials, and the Materials Research Science and Engineering Center at the University of Houston.

Literature Cited

1. Ryshkewitz E, Richerson DW. *Oxide Ceramics: Physical Chemistry and Technology*. 2nd Edition. New York, NY: Academic Press; 1985.
2. Kingery WD, Bowen HK, Uhlmann DR. *Introduction to Ceramics*. 2nd Edition. New York, NY: Wiley; 1976.
3. Vanderah TA. Talking ceramics. *Science.* 2002;298:1182-1184.
4. Valenzuela R. *Magnetic Ceramics*. Cambridge, UK: Cambridge Univ. Press; 1994.
5. Rahaman MN. *Ceramic Processing and Sintering*. 2nd Edition. New York, NY: Marcel Dekker; 2003.
6. Lee BI, Pope EJA. *Chemical Processing of Ceramics*. New York, NY: Marcel Dekker; 1994.
7. Iler RK. *The Chemistry of Silica*. New York, NY: Wiley–Interscience; 1979.
8. Brinker C, Scherer G. *Sol–Gel Science: The Physics and Chemistry of Sol–Gel Processing*. Boston, MA: Academic Press; 1990.
9. Masters K. *Spray Drying Handbook*. 4th Edition. London: George Godwin Ltd.; 1985.
10. Suresh K, Kumar NRS, Patil KC. A novel combustion synthesis of spinel ferrites, orthoferrites and garnets. *Adv Mater.* 1991;3:148-150.
11. Patil KC, Aruna ST, Ekambaram S. Combustion synthesis. *Curr Opin Solid State Mater Sci.* 1997;2:158-165.
12. Barrer RM. *Hydrothermal Chemistry of Zeolites*. London: Academic Press; 1982.
13. Tretyakov YD, Shlyakhtin OA. Recent progress in cryochemical synthesis of oxide materials. *J Mater Chem.* 1999;9:19-24.
14. Merzhanov AG. SHS technology. *Adv Mater.* 1992;4:294-295.
15. Merzhanov AG. Self-propagating high-temperature synthesis: Twenty years of research and findings. In: Munir ZA, Holt JB, eds. *Combustion and Plasma Synthesis of High-Temperature Materials*. New York, NY: VCH; 1990.
16. Munir ZA. Synthesis of high-temperature materials by self-propagating combustion methods. *Am Ceram Soc Bull.* 1988;67:342-349.
17. Puszynski JA, Majorowski S, Hlavacek V. Strongly exothermic reacting systems: Scale-up principles. *Ceram Eng Sci Process.* 1990;11:1182-1189.
18. Nersesyan MD, Avakyan PB, Martirosyan KS, Komarov AV, Merzhanov AG. Self-propagating high-temperature synthesis of ferrites. *Inorg Mater.* 1993;29:1506-1508.

19. Varma A, Rogachev AS, Mukasyan AS, Hwang S. Combustion synthesis of advanced materials: Principles and applications. *Adv Chem Eng.* 1998;24:79-226.
20. Merzhanov AG, Borovinskaya IP, Nersesian MD, Peresada AG. *Method of Manufacturing Oxide Superconductors Using Self-Propagating High-Temperature Synthesis*. U.S. Patent No. 5 064 808; 1991.
21. Lebrat JP, Varma A. Some further studies in combustion synthesis of the $YBa_2Cu_3O_{7-X}$ superconductor. *Combust Sci Technol.* 1993;88: 177-185.
22. Lin SC, Li DX, Semiat R, Richardson JT, Luss D. SHS of $YBa_2Cu_3O_{6+x}$ using large copper particles. *Physica C.* 1993;218:130-136.
23. Avakyan PB, Martirosyan KS, Mkrtchyan SO. Phase-formation during the SHS of barium ferrites. *Int J Self-Propagat High-Temp Synth.* 1992;1:551-554.
24. Avakyan PB, Nersesyan MD, Merzhanov AG. New materials for electronic engineering. *Am Ceram Soc Bull.* 1996;75:2, 50-55.
25. Martirosyan KS, Avakyan PB, Nersesyan MD. Synthesis of lead ferrite in a combustion mode. *Int J Self-Propagat High-Temp Synth.* 2001;10:193-199.
26. Martirosyan KS, Avakyan PB, Nersesyan MD. Phase-formation during self-propagating high-temperature synthesis of ferrites. *Inorg Mater.* 2002;38:400-403.
27. Ming Q, Nersesyan M, Ross K, Richardson JT, Luss D. Reaction steps and microstructure formation during SHS of $La_{0.8}Sr_{0.2}CrO_3$. *Combust Sci Technol.* 1997;128:279-294.
28. Ming Q, Nersesyan MD, Lin S, Richardson JT, Luss D. Chemical rate processes involved in SHS of $La_{0.9}Sr_{0.1}CrO_3$. *Int J Self-Propagat High-Temp Synth*. 1998;7:457-473.
29. Ming Q, Nersesyan MD, Wagner A, Ritchie J, Richardson JT, Luss D, Jacobson AJ, Yang YL. Combustion synthesis and characterization of Sr and Ga doped $LaFeO_3$. *Solid State Ionics.* 1999;122:113-121.
30. Ming Q, Nersesyan MD, Lin S, Richardson JT, Luss D, Shiryaev AA. A new route to synthesize $La_{1-x}Sr_xMnO_3$. *J Mater Sci.* 2000;35:3599-3606.
31. Grigoryan EN. SHS catalysts and support. *Int J Self-Propagat High-Temp Synth.* 1997;6:307-325.
32. Martirosyan KS, Luss D. *Carbon Combustion Synthesis of Oxides*. Provisional patent filed by University of Houston, Houston, TX; 2004.
33. Rogachev AS, Mukasyan AS, Merzhanov AG. Structural transitions in the gasless combustion of titanium–carbon and titanium–boron systems. *Dokl Phys Chem.* 1987;297:1240-1243.
34. Galwey AK, Brown ME. *Thermal Decomposition of Ionic Solids*. Amsterdam: Elsevier; 1999.
35. Hedvall JA. *Solid State Chemistry: Whence, Where and Whither*. Amsterdam: Elsevier; 1966.

Manuscript received Nov. 1, 2004, and revision received Feb. 14, 2005.